Solubility of Mixed Lanthanide Hydroxide and Oxide Solid Solutions

AUTHOR(S):

Moniruzzaman, Mohammad; Kobayashi, Taishi; Sasaki, Takayuki

CITATION:

Moniruzzaman, Mohammad ...[et al]. Solubility of Mixed Lanthanide Hydroxide and Oxide Solid Solutions. Journal of Nuclear Fuel Cycle and Waste Technology 2021, 19(3): 353-366

ISSUE DATE:

2021-09

URL:

http://hdl.handle.net/2433/276817

Research Paper

https://doi.org/10.7733/jnfcwt.2021.19.3.353

Solubility of Mixed Lanthanide Hydroxide and Oxide Solid Solutions

Mohammad Moniruzzaman, Taishi Kobayashi*, and Takayuki Sasaki
Department of Nuclear Engineering, Kyoto University, Kyotodaigaku-katsura, Nishikyo-ku, Kyoto 615-8540, Japan

(Received July 9, 2021 / Revised July 29, 2021 / Approved August 19, 2021)

The solubilities of different multicomponent lanthanide oxide (Ln_2O_3) solid solutions including binary (Ln_1 and Ln_2 = La, Nd, Eu, or Tm), ternary (Ln_1, Ln_2, and Ln_3 = La, Nd, Eu, or Tm), and higher systems (Ln = La, Ce, Pr, Nd, Sm, Eu, Gd, Tb, Dy, Ho, Er, Tm, Yb, and Lu) were studied after aging for four weeks at 60°C. Our recent study revealed that the phase transformations in binary ((La, Nd) and (La, Eu)) and ternary (La, Nd, Eu) systems are responsible for the formation of (La, Nd)$(OH)_3$, (La, Eu)$(OH)_3$, and (La, Nd, Eu)$(OH)_3$ solid solutions, respectively. The variations in the mole fractions of La^{3+}, Nd^{3+}, and Eu^{3+} in the sample solutions of these hydroxide solid solutions indicated that a thermodynamic equilibrium might account for the apparent La, Nd, and Eu solubilities. Conversely, the binary and ternary systems containing Tm_2O_3 as the heavy lanthanide oxide retained the oxide-based solid solutions, and their solubility behaviors were dominated by their congruent dissolutions. In the higher multicomponent system, the X-ray diffraction patterns of the solid phases, before and after contact with the aqueous phase indicated the formation of a stable oxide solid solution and their solubility behavior was explained by its congruent dissolution.

Keywords: Lanthanide, Oxide Hydroxide, Solid solution, Solubility

*Corresponding Author.
Taishi Kobayashi, Kyoto University, E-mail: kobayashi@nucleng.kyoto-u.ac.jp, Tel: +81-75-383-3919

ORCID
Mohammad Moniruzzaman http://orcid.org/0000-0002-9644-6036
Taishi Kobayashi http://orcid.org/0000-0001-9094-2509
Takayuki Sasaki http://orcid.org/0000-0002-0452-8211

1. Introduction

During the safety assessment of radioactive waste disposal, it is valuable to predict the solubility limits of radionuclides (RNs) under disposal conditions. Thus, the solubility limit of each RN has been investigated, as reported in numerous literature and thermodynamic databases established based on the comprehensive reviews of data [1-4]. Among the different RNs, lanthanides are fission products that are accumulated in radioactive waste, show similar physico-chemical behavior owing to their comparable ionic radius with trivalent actinides such as americium and curium in a natural geochemical system. Since handling of macro amount of Am/Cm is difficult in laboratories, trivalent lanthanides (Ln(III)) have been used as analogs of these α-emitting actinides. Without any complexing ligand, the solubility limits of lanthanides are primarily controlled by their oxides or hydroxides [5-7]. Studies have revealed that lanthanide phosphates can easily form solid solutions because of their similarity to the lanthanide series [8, 9], and our previous study revealed that the formation of binary and ternary solid solutions of oxides and hydroxides depended on the experimental conditions and combination of the elements [10]. Thus, the solubility limits of pure lanthanide oxides or hydroxides, as well as their solid solutions, would be interesting and valuable for elucidating the solubility limits of lanthanides. Since the migration behavior of trivalent lanthanides and actinides is primarily dependent on their low solubilities, the mechanisms need to be quantitatively understood based on thermodynamics.

The literature extensively reports the solubility behavior of solid solutions in aqueous solutions, and their thermodynamic description is established employing the Lippman diagram [11-15]. The theory effectively explains the solubility of binary solid solutions, such as alkaline earth sulfates, carbonates, and halides [13, 14], in aqueous solutions. Compared with the abundant studies on the alkaline earth elements, only a few reports are available on the investigations of the systems between lanthanide solid and aqueous solutions [16]. Additionally, only a few studies have explored the incorporation of Eu(III) in calcite in aqueous systems [17, 18], although there is almost no report regarding the solubility of lanthanide oxide or hydroxide solid solutions in aqueous solutions. As aforementioned, several binary and ternary lanthanide (La, Nd, Eu, and Tm) oxide solid solutions have been synthesized by our group, and their transformations into hydroxide solid solutions based on the combination of the lanthanide series were observed [10]. As a single oxide, lighter lanthanide oxides, such as La_2O_3, can be readily converted into a hydroxide ($La(OH)_3$), while heavier lanthanide oxides (Tm_2O_3) are not [6, 19]. The phase transformations involving binary and ternary lanthanide oxide solid solutions in aqueous solutions are well-explained by the combination of the tendencies observed in single oxides [10]. This study focuses on the solubility of the binary and ternary solid solutions of lanthanide oxides and hydroxides. Here, an oxide solid solution containing all the lanthanide elements, except Pm, was prepared and allowed to contact an aqueous solution to investigate the solubility and solid phase following the immersion. The solubility behaviors of the single-to-binary, ternary, and multicomponent lanthanide oxides and hydroxides, as well as the characterizations of the solid phases, were also discussed.

2. Experimental

2.1 Materials

Reagent grades of sodium perchlorate monohydrate ($NaClO_4 \cdot H_2O$, 98%), nitric acid (HNO_3, 60%), perchloric acid ($HClO_4$, 60%), sodium hydroxide (NaOH, 97%), and polyvinyl alcohol (PVA 3500, 78% hydrolyzed) were purchased from Wako Pure Chem. HEPES ($C_8H_{18}N_2O_4S$, 99.0%; Dojindo) was employed to adjust the pH of the sample solutions to the neutral. The lanthanide oxides (La_2O_3 (99.99%), $Ce(NH_4)_2(NO_3)_6$ (95.0%), Pr_2O_3 (99.9%),

Nd_2O_3 (99.9%), Sm_2O_3 (99.9%), Eu_2O_3 (99.9%), Gd_2O_3 (99.9%), Tb_2O_3 (99.9%), Dy_2O_3 (99.9%), Ho_2O_3 (99.9%), Er_2O_3 (99.9%), Tm_2O_3 (99.9%), Yb_2O_3 (99.9%), and Lu_2O_3 (99.5%)) were purchased from Wako Pure Chemical Industries. Due to an insolubility of CeO_2, $Ce(NH_4)_2(NO_3)_6$ was used as a source to prepare Ce(IV) stock solution. Purified deionized water (Milli-Q, Millipore) was employed for the preparations of all the solutions. The syntheses of the solid phases, as well as the preparations and measurements of the sample solutions, were performed at atmospheric pressure and 25°C. The hydrogen ion concentration (pH_c) values of the sample solutions were measured by a pH meter (D-72, Horiba Ltd.) employing a combined glass electrode (9615-10D, Horiba Ltd.). The reference electrode was filled with 3.6 M NaCl and 0.4 M $NaClO_4$ (Wako Pure Chem.), and the experimental pH values (pH_{exp}) of standard $HClO_4$ and NaOH solutions (pH_c 1, 2, 3, 11, 12, and 13; Wako Pure Chem.) at I = 0.1 M utilizing $NaClO_4$ at 25°C were recorded. Based on the linear approximation of pH_{exp} and pH_c for the standard solutions, pH_c value for each sample solution was obtained.

2.2 Sample Preparation

Three binary mixed oxides, $(La, Nd)_2O_3$, $(La, Eu)_2O_3$, and $(Eu, Tm)_2O_3$; two ternary mixed oxides, $(La, Nd, Eu)_2O_3$ and $(La, Eu, Tm)_2O_3$; and one multicomponent mixed oxide, Ln_2O_3 (Ln = La, Ce, Pr, Nd, Sm, Eu, Gd, Tb, Dy, Ho, Er, Tm, Yb, and Lu) were synthesized via a polymeric steric entrapment method [20, 21]. The detailed procedures for synthesizing the binary and ternary mixed oxides have been described elsewhere [10]. Ln (Ln = La, Nd, Eu, and Tm) nitrate stock solutions with Ln concentration ([Ln] = 0.3 M) were prepared by dissolving each La_2O_3, Nd_2O_3, Eu_2O_3, and Tm_2O_3 in HNO_3. Further, aliquots of two or three stock solutions were mixed at certain molar ratios and added to an equivalent molar ratio of 5wt% PVA stock solution [10]. Regarding the multicomponent mixed oxide, an equal volume of each Ln stock solution ([Ln] = 0.3 M) was mixed and added to an equivalent molar ratio of the 5wt% PVA stock solution. The resulting binary, ternary, and multicomponent oxide solutions were stirred for 1 h employing a magnetic stirrer, after which it was heated for ~2 h at 200°C. After drying, the solids were crushed in a mortar and further heated in a muffle furnace (FO-100, Yamato Scientific Co.) for 4 h at 1,000°C. For comparison, mixtures of the pure oxides were prepared without heating.

2.3 Solubility Experiment

The synthesized binary, ternary, and multicomponent mixed oxides, as well as the mixtures of pure oxides, were utilized as the initial solid phases in the solubility experiment. The experimental procedure followed that of our previous study for single lanthanide oxides [19]. Briefly, a certain amount of a 0.1 M $NaClO_4$ solution containing 0.01 M HEPES as its pH buffer was prepared as an initial solution, and pH_c was adjusted with 0.1 M $HClO_4$ and 0.1 M NaOH to maintain a constant ionic strength (I) (I = 0.1 M). Each aliquot (12 mL) was withdrawn at fixed pH levels ranging from pH_c 7–10 and placed in polypropylene tubes. Thereafter, the mixed oxides or mixtures of the pure oxides (~20 mg) were added into the sample tubes to obtain a maximum Ln concentration of ~0.01 M in each tube when the additional solid phase was completely dissolved. Regarding the selected samples, the solid phases (120 mg) were added into 100 mL of the sample solutions at pH 8.2 and 9.7 for the X-ray diffraction (XRD) analysis after the solubility experiment. After the preparation, the caps of the sample tubes were closed tightly, and the sample tubes were placed in a temperature chamber (ETTAS E0450B, AS ONE Co.), which was controlled at the aging temperatures (T_{age} = 60°C). The sample tubes were periodically hand-shaken for a few minutes during aging for up to four weeks.

After the aging at 60°C, the sample tubes were removed from the chamber and placed in thermostatted baths, which were maintained at a measurement temperature (T_{meas}) (T_{meas} = 25°C) and kept for a few days. As previously described

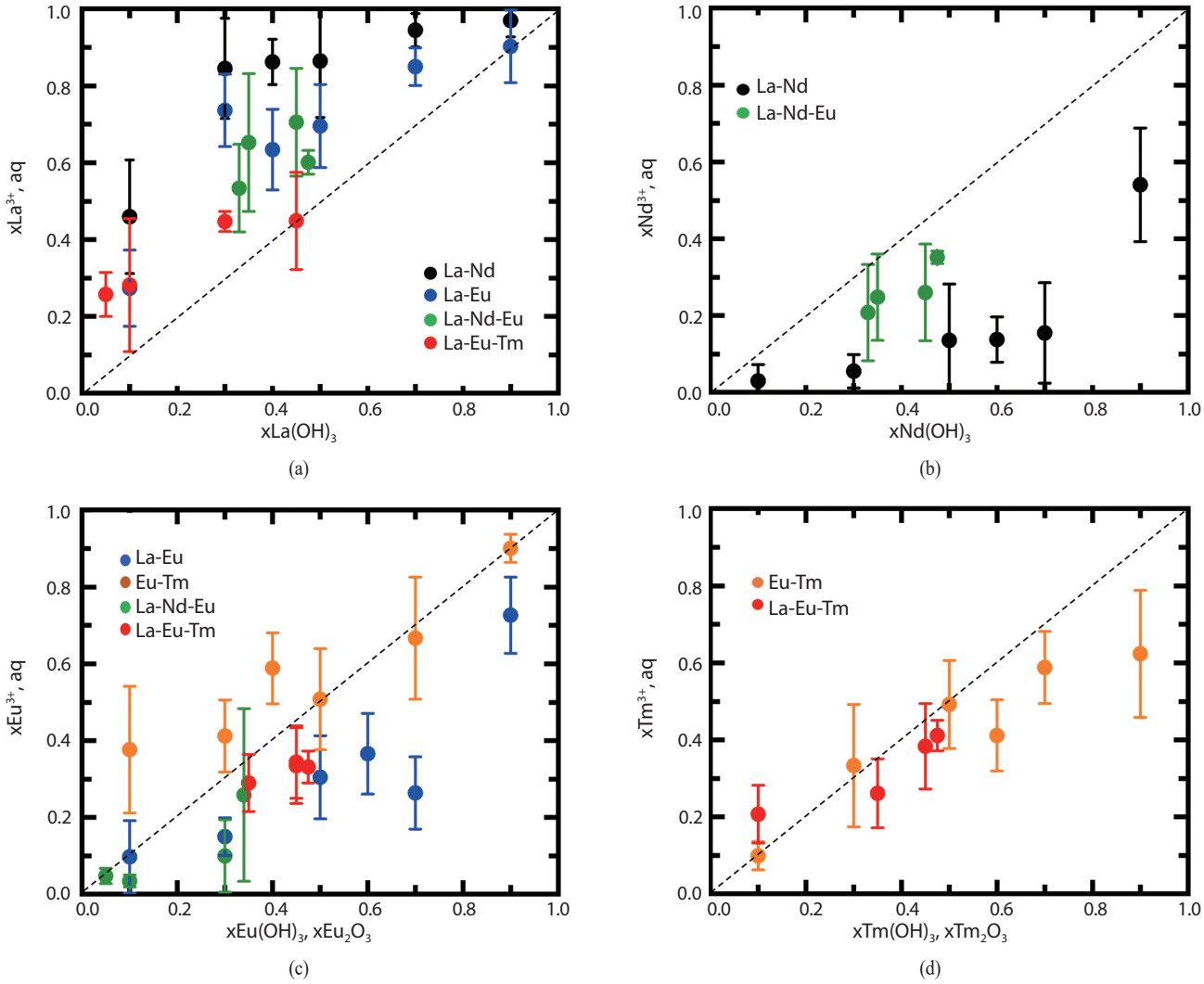

Fig. 1. Mole fraction of Ln^{3+} ($x_{Ln^{3+},aq}$) in the sample solutions as a function of the mole fraction of $Ln(OH)_3/Ln_2O_3$ in the solid phases ($x_{Ln(OH)_3}, x_{Ln_2O_3}$) (Ln = (a) La, (b) Nd, (c) Eu, and (d) Tm). The dotted line in the figures represent the congruent dissolution, $x_{Ln^{3+},aq} = x_{Ln(OH)_3}, x_{Ln_2O_3}$.

[19], the supernatants (0.5 mL) were filtered through the ultrafiltration membranes (3 kDa; Microcon, Millipore) at 25°C. Afterward, 0.3 mL of the filtrate was collected and acidified employing 2.0 mL of 0.1 M HNO_3. Afterward, the Ln concentrations were measured via inductively coupled plasma mass spectrometry (ICP-MS; ELANDRC II, PerkinElmer). The detection limit was ~10^{-9} M for each element, and the standard error was within 10% for each measurement ICP-MS measurement, resulting in ± 0.1 in the log units of the Ln concentrations. Notably, the acquisition of three different supernatants from a certain sample tube yielded a maximum scattering (log [Ln]) of ± 0.5.

The solid phases of the multicomponent mixed oxides and mixtures of the pure oxides were characterized before and after the solubility experiments. Afterward, the solid phase was separated by centrifugation (H-103N, Kokusan) for 5 min at 5,000 rpm and dried in a vacuum desiccator. The diffraction patterns of the solid phase were obtained

Table 1. Summary of the binary and ternary solid phases before and after the solubility experiment

System	Subsystem	Mixing molar ratio	Crystal phase	
			Before solubility exp.	After solubility exp.
Binary	$(La, Nd)_2O_3$	La:Nd = 9:1–1:9	Complete SS (trigonal)	Complete SS (hexagonal)
	$(La, Eu)_2O_3$	La:Eu = 9:1–1:9	La_2O_3 and Eu_2O_3 based SS (trigonal, cubic)	Complete SS (hexagonal)
	$(Eu, Tm)_2O_3$	Eu:Tm = 9:1–1:9	Separated SS (cubic)	$Eu(OH)_3$ and Tm_2O_3 based SS (hexagonal and cubic)
Ternary	$(La, Nd, Eu)_2O_3$	La:Nd:Eu= 4.75:4.75:0.5 –3.5:3.5:3.0	Separated SS (trigonal, cubic and monoclinic)	Complete SS (hexagonal)
	$(La, Eu, Tm)_2O_3$	La:Eu:Tm= 0.5:4.75:4.75 –4.5:4.5:1	Separated SS (trigonal, cubic and monoclinic)	$(La, Eu)(OH)_3$ and $(Eu, Tm)_2O_3$ based SS (hexagonal and cubic)

via XRD (Miniflex, Rigaku) utilizing Cu-Kα radiation (λ = 0.154 nm) in the scattering angle range, 2θ = 10°–60°, and at a scan rate of 5°/min. The solid phases of the binary and ternary lanthanide oxides were analyzed before and after the solubility experiments in the previous study [10].

3. Results and Discussion

3.1 Binary and Ternary Solid Solutions of Lanthanide Hydroxide

Our previous study revealed that a complete solid solution of the synthesized $(La, Nd)_2O_3$ was transformed into a complete solid solution of $(La, Nd)(OH)_3$ in the sample solution during the aging for four weeks at 60°C as confirmed by the XRD patterns of the solid phases [10]. Regarding the (La, Eu) and (La, Nd, Eu) systems, although the separated oxide phases were observed in the synthesized $(La, Eu)_2O_3$ and $(La, Nd, Eu)_2O_3$ depending on the mixing ratio, the formations of single complete solid solutions of $(La, Eu)(OH)_3$ and $(La, Nd, Eu)(OH)_3$ were confirmed after the aging in the sample solutions at 60°C [10]. Here, the solubilities of these binary and ternary hydroxide solid solutions were measured at 25°C after removing the sample solution from the oven and keeping them for a few days at 25°C. To observe a steady-state, the solubilities of the selected samples were measured again after settling at different durations of 4 to 12 weeks at 25°C. The absence of a significant difference between the solubility values at different settling times indicated that the steady-state was achieved. Similarly, the steady-state of solubility data was also observed for the single lanthanide oxides and hydroxides after several weeks [19]. Thus, the solubility data after 4 weeks of aging were used for further analysis in the present study.

In the pH_c range of 7.0 < pHc < 8.5, Ln^{3+} and $LnOH^{2+}$ (Ln = La, Nd, and Eu) were considered as the dominant soluble species based on their hydrolysis constants [7]. Thus, the concentration of Ln^{3+} was calculated from the obtained solubility by subtracting the concentration of $LnOH^{2+}$ employing the reported hydrolysis constants. Thereafter, the mole fractions of La^{3+}, Nd^{3+}, and Eu^{3+} in each sample solution ($x_{La^{3+},aq}$, $x_{Nd^{3+},aq}$, and $x_{Eu^{3+},aq}$, respectively) were calculated as $x_{Ln^{3+},aq}=[Ln^{3+}]/\sum([Ln^{3+}])$. Fig. 1 shows the average values of (a) $x_{La^{3+},aq}$, (b) $x_{Nd^{3+},aq}$, and (c) $x_{Eu^{3+},aq}$ for a certain $x_{Ln(OH)_3}$ within the pH_c range of 7.0 < pH_c < 8.5. $x_{Ln(OH)_3}$ represents the mole fraction of each hydroxide in the solid solutions and corresponds to the Ln mixing ratio during the preparation of the sample based on the characterization of the solid phase of the solid solutions in ref. [10].

Regarding $(La, Nd)(OH)_3$, $x_{La^{3+},aq}$ increased with the

increasing $x_{La(OH)_3}$; it was larger than, $x_{La(OH)_3}$. $x_{Nd^{3+},aq}$ increased with the increasing $x_{Nd(OH)_3}$ and was less than $x_{Nd(OH)_3}$ (Figs. 1(a) and (b)). Further, $x_{La^{3+},aq}$ was constant (0.99), as calculated from the solubility products of $La(OH)_3$ (log K = −21.7, I = 0.1 [19]) and $Nd(OH)_3$ (log K = −23.5, I = 0.1 [22]) when the separated $La(OH)_3$ and $Nd(OH)_3$ were the solubility-limiting solid phases for the solubilities of La and Nd. Since the experimental values of $x_{La^{3+},aq}$ and $x_{Nd^{3+},aq}$ were not constant (they depended on $x_{La(OH)_3}$and $x_{Nd(OH)_3}$ rather than the separated $La(OH)_3$ and $Nd(OH)_3$), the (La, Nd)$(OH)_3$ solid solution was probably accountable for the apparent solubilities of La and Nd. Conversely, since the experimental values $x_{La^{3+},aq}$ were plotted in the region at $x_{La^{3+},aq} > x_{La(OH)_3}$, a congruent dissolution ($x_{La^{3+},aq} = x_{La(OH)_3}$) did not seem to dominate the solubility of (La, Nd)$(OH)_3$ under the investigated experimental conditions. Notably, $(La, Nd)_2O_3$ (the initial phase in the solubility experiment) was converted into (La, Nd) $(OH)_3$ during the four weeks of aging in the sample solution at 60°C as shown in Table 1. After a possible initial congruent dissolution, the system could attain a certain thermodynamic equilibrium between (La, Nd)$(OH)_3$ and (La^{3+}, Nd^{3+}) in the sample solutions. Additional discussion is presented in the following section.

Regarding (La, Eu)$(OH)_3$, the $x_{La^{3+},aq}$ value increased with the increasing value of $x_{La(OH)_3}$; it was found within the region of $x_{La^{3+},aq} > x_{La(OH)_3}$. Further, the obtained $x_{Eu^{3+},aq}$ was lesser than $x_{Eu(OH)_3}$, although the values of $x_{La^{3+},aq}$ and $x_{Eu^{3+},aq}$ were relatively scattered (Figs. 1(a) and (c)). Further, $x_{La^{3+},aq}$ could be a constant that was calculated from the solubility products of separated $La(OH)_3$ (log K = −21.7, I = 0.1 [19]) and $Eu(OH)_3$ (log K = −24.3, I = 0.1 [7]) if separated $La(OH)_3$ and $Eu(OH)_3$ were the solubility-limiting phases. Similar to the (La, Nd)$(OH)_3$ system, it is possible that the incongruent dissolution/precipitation of the (La, Eu)$(OH)_3$ solid solution rather than separated $La(OH)_3$ and $Eu(OH)_3$ phases accounted for the apparent solubilities of La and Eu. Notably, the $x_{La^{3+},aq}$ values of (La, Eu)$(OH)_3$ were slightly lower than those of (La, Nd) $(OH)_3$. Although the bulk structure of (La, Eu)$(OH)_3$, as confirmed by the XRD patterns, was a complete solid solution, and their subsequent analysis (the initial material of the (La, Eu) system) was separated into La_2O_{3-} and Eu_2O_{3-} based solid solutions [10]. When the initial material was separated into pure La_2O_3 and Eu_2O_3, Eu_2O_3 retained its stability as the oxide after aging for four weeks at 60°C [10]. If small portions of Eu_2O_3 existed in (La, Eu)$(OH)_3$, the $x_{Eu^{3+},aq}$ values would increase since Eu_2O_3 was more soluble than $Eu(OH)_3$ [7, 19]; hence, the $x_{La^{3+},aq}$ values of (La, Eu)$(OH)_3$ might be underestimated.

Regarding the ternary solid solutions of (La, Nd, Eu)$(OH)_3$, their $x_{La^{3+},aq}$ values were also above the line, $x_{La^{3+},aq} = x_{La(OH)_3}$ and $x_{Nd^{3+},aq}$; the values of $x_{Eu^{3+},aq}$ were less than $x_{Nd(OH)_3}$ and $x_{Eu(OH)_3}$, respectively, (Figs. 1(a), (b), and (c)). As shown in Table 1, the initial solid phases consisting of the separated oxide solid solutions, (La, Nd, $Eu)_2O_3$ were transformed into a single complete solid solution of (La, Nd, Eu)$(OH)_3$ [10]. Owing to the possible effect of the residual Eu_2O_3, the $x_{La^{3+},aq}$ and $x_{Eu^{3+},aq}$ values of (La, Nd, Eu)$(OH)_3$ were obtained close to those of (La, Eu)$(OH)_3$. The incongruent dissolution/precipitation of the (La, Nd, Eu)$(OH)_3$ solid solution might control the apparent solubilities of La, Nd, and Eu through the solid-phase transformation process, as in binary (La, Nd)$(OH)_3$ and (La, Eu)$(OH)_3$.

3.2 Binary and Ternary Solid Solutions of Lanthanide Oxide

Regarding the binary Eu–Tm and ternary La–Eu–Tm systems, as shown in Table 1, their solid phases after contacting the aqueous sample solutions were not complete hydroxide solid solutions because Tm_2O_3, which is a heavy lanthanide oxide, was not readily transformed into $Tm(OH)_3$ [6, 10, 19]. Regarding the Eu–Tm system, the solid phase, following the immersion, was a mixture of $Eu(OH)_{3-}$ and Tm_2O_{3-} based solid solutions depending on the Eu–Tm mixing ratio [10]. Regarding the ternary

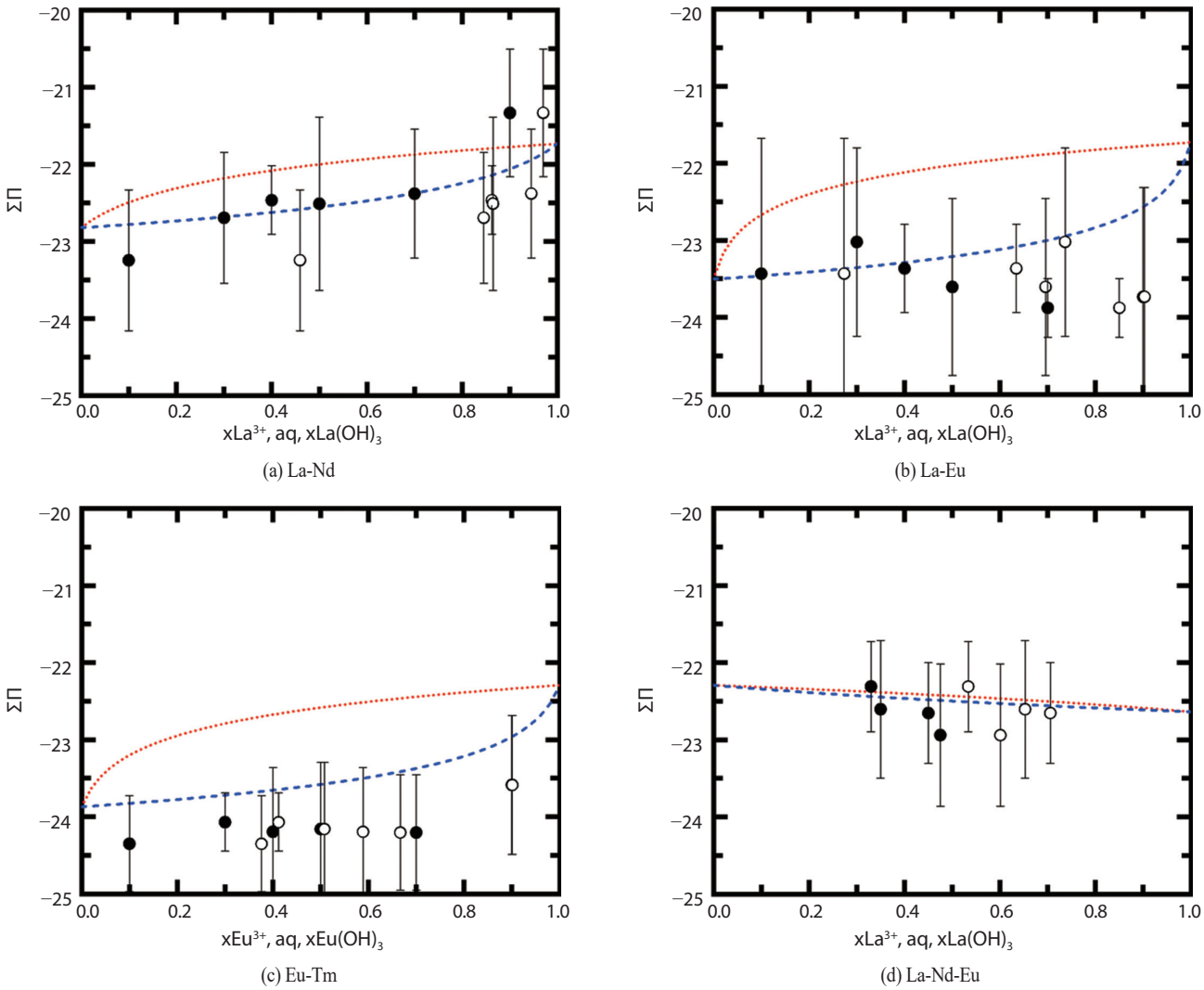

Fig. 2. Lippmann diagram of the (a) $(La, Nd)(OH)_3$, (b) $(La, Eu)(OH)_3$, (c) $(Eu, Tm)_2O_3$, and (d) $(La, Nd, Eu)(OH)_3$ solid solutions at 25°C after aging for four weeks at 60°C in 0.1 M $NaClO_4$ solutions. The open symbols represent ΣΠ against $x_{Ln^{3+},aq}$ in the solutions, and the filled symbols represent ΣΠ against $x_{Ln(OH)_3}$ or $x_{Ln_2O_3}$ in the solid solutions. The dotted and broken lines show the solidus and solutus curves, which were calculated from the reported hydrolysis constants of the endmembers [7,19,23].

La–Eu–Tm system, the solid phase was a mixture of $(La, Eu)(OH)_3$– and $(Eu, Tm)_2O_3$– based solid solutions [10]. Considering that the dominant soluble species were Ln^{3+} and $LnOH^{2+}$ (Ln = La, Eu, and Tm) in the pH_c range of $7.0 < pH_c < 8.5$, the Ln^{3+} concentration was calculated from the obtained solubility by subtracting that of $LnOH^{2+}$ employing the reported hydrolysis constants [7]. Thereafter, the mole fractions ($x_{La^{3+},aq}$, $x_{Eu^{3+},aq}$, and $x_{Tm^{3+},aq}$) were calculated from the Ln^{3+} concentrations and plotted (Fig. 1) as functions of $x_{Ln(OH)_3}$ or $x_{Ln_2O_3}$ in the total solid phase. Regarding the binary Eu–Tm system, Eu and Tm existed in two separate phases, i.e., the $Eu(OH)_3$– and Tm_2O_3– based solid solutions at Eu:Tm = 7:3 and 5:5, respectively, while Eu was incorporated in Tm_2O_3 at Eu–Tm = 4:6, 3:7, and 1:9 [10]. Since the lattice parameter of $Eu(OH)_3$ was constant and the same as that of pure $Eu(OH)_3$, it was challenging to

incorporate Tm into the $Eu(OH)_3$ structure [10]. The values of $x_{Tm^{3+},aq}$ were observed along the $x_{Tm^{3+},aq} = x_{Tm_2O_3}$ line (Fig. 2(d)), indicating the congruent dissolution of Tm from the Tm_2O_{3-} based solid solutions. Conversely, Eu existed in the $Eu(OH)_{3-}$ and Tm_2O_{3-} based solid solutions. Since the solubility of Tm_2O_3 was approximately one order of magnitude higher than that of $Eu(OH)_3$ according to their solubility products [6, 10, 19], the dissolution of the Tm_2O_{3-} based solid solution proceeded congruently and might have dominated the apparent Eu solubility. The solubility of Tm in the ternary La–Eu–Tm system could be similarly explained. $x_{La^{3+},aq}$ was observed to be slightly larger than $x_{La(OH)_3}$, and $x_{Eu^{3+},aq}$ was slightly lower than $x_{Eu(OH)_3}$ in the ternary system. Regarding the analysis of the solid phase, La and Eu formed a hydroxide solid solution separately from Tm_2O_3. The observed trends of $x_{La(OH)_3}$ and $x_{Eu^{3+},aq}$ were similar to that of $(La, Eu)(OH)_3$.

3.3 Discussion on the Solubilities of the Binary and Ternary Solid Solutions

Regarding the solubilities of the binary solid solutions, different studies have considered their thermodynamic analyses; the Lippmann phase-diagram theory is known to adequately explain the experimental data of many systems [13, 14, 23]. Employing this theory, the total solubility product (ΣΠ) of lanthanide oxide/hydroxide solid solutions ($(L_1, L_2)(OH)_3$ or $(L_1, L_2)_2O_3$ (L_1, L_2 = La, Nd, Eu, and Tm)) could be defined, as follows:

$$\Sigma\Pi = ([L_1^{3+}] + [L_2^{3+}])[OH^-]^3 , \quad (1)$$

Considering that $(L_1, L_2)(OH)_3$ or $(L_1, L_2)_2O_3$ was an ideal solid solution in the whole range of their mole fractions, ΣΠ of $(L_1, L_2)(OH)_3$ or $(L_1, L_2)_2O_3$ could be expressed employing the solubility products of the endmembers and mole fractions in the solid phase (Eq. 2) or solutions (Eq. 3). For instance, the ΣΠ of $(L_1, L_2)(OH)_3$ is described by the following:

$$\Sigma\Pi = K_{L_1(OH)_3} \cdot x_{L_1(OH)_3} + K_{L_2(OH)_3} \cdot x_{L_2(OH)_3} \quad (2)$$

$$\Sigma\Pi = \frac{1}{\left(\frac{x_{L_1^{3+},aq}}{K_{L_1(OH)_3}} + \frac{x_{L_2^{3+},aq}}{K_{L_2(OH)_3}}\right)} , \quad (3)$$

where $K_{L_1(OH)_3}$ and $K_{L_2(OH)_3}$ are the solubility products of pure $L_1(OH)_3$ and $L_2(OH)_3$, respectively.

The experimental ΣΠ values of $(La, Nd)(OH)_3$, $(La, Eu)(OH)_3$, and $(Eu, Tm)_2O_3$ are plotted in Figs. 2(a), 2(b), and 2(c), respectively, as functions of the mole fractions of the solids and solutions, as well as the calculated solidus and solutus curves, based on Eq. (2) and (3), respectively. As discussed above, the solubility values ([Ln]) in the pH_c range of $7.0 < pH_c < 8.5$ were used to calculate $[Ln^{3+}]$ and then obtain average ΣΠ values based on in Eq. (1) for different pH_c conditions.

Although each plot reveals a relatively large uncertainty, the trend of ΣΠ values of $(La, Nd)(OH)_3$ observed to be comparable with the calculated curves with a little downward shift. This probably confirms that $(La, Nd)(OH)_3$ was in a thermodynamic equilibrium with La^{3+} and Nd^{3+} in the sample solutions. Regarding the lattice parameters of $(La, Nd)(OH)_3$, it was considered that the La–Nd composition of the solid phase did not change during the transformation of $(La, Nd)_2O_3$ into $(La, Nd)(OH)_3$ [10]. Therefore, after the probable direct solid-phase transformation into $(La, Nd)(OH)_3$, the solid phase appeared to thermodynamically control the solubilities of La and Nd. Conversely, the ΣΠ values of $(La, Eu)(OH)_3$ did not agree well with the calculated solidus and solutus curves of $(La, Eu)(OH)_3$. The experimental ΣΠ values were observed to be almost constant despite of large uncertainties against $x_{La^{3+},aq}$ and $x_{La(OH)_3}$, although the calculate ones indicated an increase of ΣΠ values with increasing amount of La ratio. As aforementioned, the probable existence of small portions of the residual Eu_2O_3 might contribute to the mole fractions of

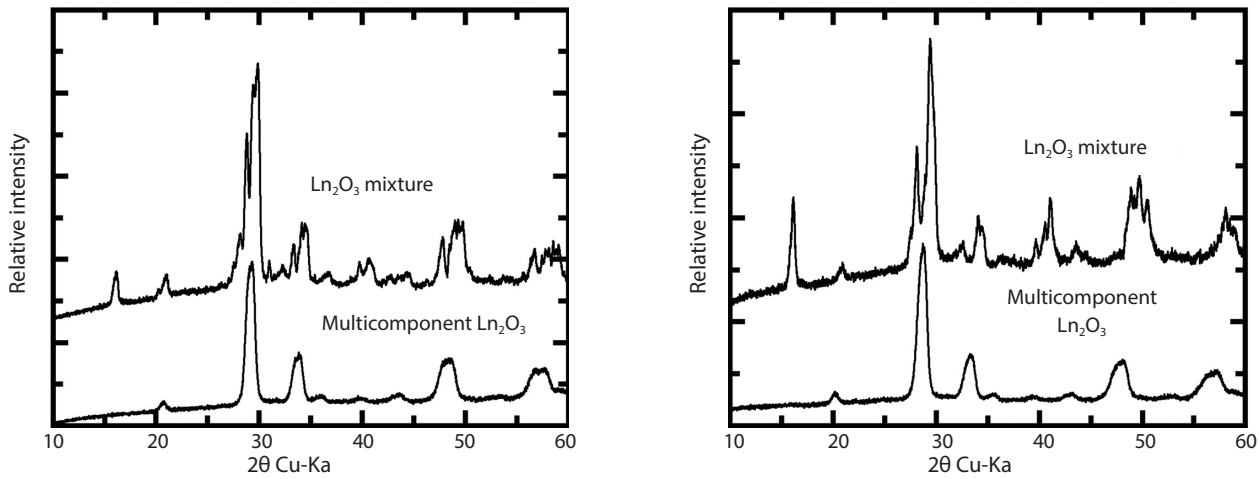

Fig. 3. XRD patterns of the multicomponent Ln_2O_3 (Ln = La – Lu) (a) before and (b) after contacting the aqueous solution for four weeks at 60°C, as well as the mixture of the separated pure oxides.

the solids and solutions. The solid-phase analysis of the initial $(La, Eu)_2O_3$ revealed that La was barely dissolved in Eu_2O_3, indicating that $x_{La(OH)_3}$ might be larger in $(La, Eu)(OH)_3$ if the residual Eu_2O_3 remained after the aging period during the solubility experiment. However, this could not explain the deviation of the experimental plots from the calculated curves. The solubility of La in $(La, Eu)(OH)_3$ decreased rapidly with a small amount of coexisting Eu in the system. However, further investigation is required to clarify the trend of the ΣΠ values of $(La, Eu)(OH)_3$. Conversely, the ΣΠ values for $(Eu, Tm)_2O_3$ were much lower than the calculated solidus and solutus curves of the Eu_2O_3–Tm_2O_3 system and appeared to be almost constant against $x_{Eu_2O_3}$, further supporting the congruent dissolution of $(Eu, Tm)_2O_3$, where $([Eu^{3+}] + [Tm^{3+}])$ in Eq. (1) was constant.

Regarding the ternary La–Nd–Eu system, the three elements formed a single $(La, Nd, Eu)(OH)_3$ solid solution. Since the investigated La:Nd:Eu ratio included 0.475:0.475:0.050, 0.45:0.45:0.10, and 0.35:0.35:0.30, the present ternary system was treated as a quasibinary system along with a combination of $(La_{0.5}, Nd_{0.5})(OH)_3$ and $Eu(OH)_3$ to apply the Lippmann phase diagram to these systems. Fig. 2(d) shows the experimental ΣΠ values of $(La, Nd, Eu)(OH)_3$ as functions of $x_{La^{3+},aq}$ and $x_{La(OH)_3}$ together with the calculated solidus and solutus curves. The experimental and calculated results probably correlated, although the solubility products of the endmembers, $(La_{0.5}, Nd_{0.5})(OH)_3$ and $Eu(OH)_3$, were similar. Notably, the solubility product of $(La_{0.5}, Nd_{0.5})(OH)_3$ was obtained from those of $La(OH)_3$ and $Nd(OH)_3$ employing Eq. (2). The solubility product of $(La_{0.5}, Nd_{0.5})(OH)_3$ was calculated to be $\log K = -22.6$ from the solubility products of $La(OH)_3$ ($\log K = -21.7$) and $Nd(OH)_3$ ($\log K = -23.5$), which happened to be close to that of $Eu(OH)_3$ ($\log K = -22.3$).

Thus, the solubilities of the binary and ternary solid solutions of lanthanide hydroxides might be controlled via a thermodynamic equilibrium of the hydroxide solid solutions with Ln^{3+}. Contrarily, the solid solutions of the lanthanide oxides might be controlled by congruent dissolution. The system containing Tm_2O_3 as the heavy lanthanide oxide retained its oxide-based solid solution, while that containing only the light lanthanide oxides was readily transformed into the hydroxide solid solution. These trends could be related to the solubilities of the binary and ternary lanthanide oxide/hydroxide systems.

3.4 Solid-phase and Solubility of the Multicomponent Ln_2O_3 (1:1) Mixed System

3.4.1 Solid-phase Characterizations Before and After the Solubility Experiment

Fig. 3(a) shows the XRD patterns of the multicomponent Ln_2O_3 (Ln = La – Lu) mixed oxide before it contacted the sample solution, as well as that of the mixture of the separated pure oxides. Employing the polymeric steric entrapment method, the diffraction peaks of the synthesized Ln_2O_3 mixed oxide were characterized employing the typical peaks of the cubic phase (Ia-3), which are often detected in medium to heavy Ln_2O_3. Considering the absence of a peak of the trigonal phase (P-3m1) at $2\theta = 15°$, which is typical for light Ln_2O_3, such as La_2O_3 and Nd_2O_3 [10], and the smooth shape of each peak compared with that of the mixture of pure oxides, it is assumed that the mixed oxide formed a cubic-based oxide solid solution. In the binary system, $(La, Nd)_2O_3$, the peaks of the synthesized solid solution corresponded to those of the trigonal phase, while the binary system, $(La, Eu)_2O_3$, resulted in the trigonal and cubic separated phases [10]. Owing to the inclusion of a series of light and heavy lanthanides in the solid-phase synthesis, the lighter lanthanides might not separate; they might be dissolved into heavier cubic-phase Ln_2O_3.

Fig. 3(b) shows the XRD patterns of the multicomponent Ln_2O_3 mixed oxide, as well as the mixture of pure oxides after aging for four weeks at 60°C. In the XRD pattern of the mixture of pure oxides, an increase in the relative intensity at $2\theta = 15°$ was attributed to the transformation of light Ln_2O_3 into $Ln(OH)_3$ exhibiting a hexagonal phase (P63/m), as observed in the mixtures of (La_2O_3 + Nd_2O_3), (La_2O_3 + Eu_2O_3), and (La_2O_3 + Nd_2O_3 + Eu_2O_3) [10]. The remaining peaks observed to be similar to those of before aging, indicating no solid solution formation. Conversely, no peak was observed in the XRD pattern of the multicomponent Ln_2O_3 mixed oxide at $2\theta = 15°$ after aging in the sample solution at 60°C, indicating that there was no solid-phase transformation of the light Ln_2O_3 into $Ln(OH)_3$ probably because of the incorporation of the light lanthanides into the heavier Ln_2O_3 to form a solid solution, which is stable and cannot be transformed into $Ln(OH)_3$; thus, the light lanthanides might be stabilized as Ln_2O_3. Therefore, the solid solution of the multicomponent Ln_2O_3 could be mixed oxide remained during the solubility experiment. The inclusion of a series of light to heavy lanthanides in multicomponent mixed oxide samples is the most different point compared to the binary and ternary phases as discussed in [10], where separated two or three elements are included to prepare the solid phases. Since the lighter lanthanides dissolved into heavier cubic-phase Ln_2O_3 in multicomponent mixed oxide samples, the lighter lanthanides might not transformed to the hydroxides.

Table 2. Mole fraction of each lanthanide in the multicomponent Ln_2O_3 mixed oxide and separated pure oxides/hydroxides

	Multicomponent Ln_2O_3 mixed oxide	Separated pure oxides/hydroxides	$Ln(OH)_3$, $I = 0$ [7]
Element	Mole fraction	Mole fraction	log K
La	0.047 ± 0.029	0.280 ± 0.109	−22.28 ± 0.34
Ce	0.004 ± 0.003	0.000 ± 0.000	−23.5 ± 0.5
Pr	0.039 ± 0.017	0.175 ± 0.058	−23.4 ± 0.2
Nd	0.102 ± 0.085	0.049 ± 0.032	−24.11 ± 0.09
Sm	0.061 ± 0.042	0.025 ± 0.015	−24.8 ± 0.3
Eu	0.050 ± 0.017	0.058 ± 0.044	−25.52 ± 0.30
Gd	0.053 ± 0.023	0.075 ± 0.020	−24.80 ± 0.58
Tb	0.052 ± 0.015	0.077 ± 0.012	−25.67 ± 0.30
Dy	0.073 ± 0.015	0.060 ± 0.028	−25.74 ± 0.30
Ho	0.100 ± 0.026	0.060 ± 0.030	−26.4 ± 0.3
Er	0.126 ± 0.023	0.039 ± 0.024	−26.21 ± 0.30
Tm	0.100 ± 0.045	0.020 ± 0.016	−26.44 ± 0.40
Yb	0.095 ± 0.037	0.016 ± 0.012	−26.65 ± 0.20
Lu	0.112 ± 0.040	0.021 ± 0.013	−26.57 ± 0.20

3.4.2 Solubility of the Multicomponent Ln_2O_3 Mixed Oxide

Figs. 4(a) and 4(b) show the solubilities of the Ln series of the mixture of the separated pure oxides, as well

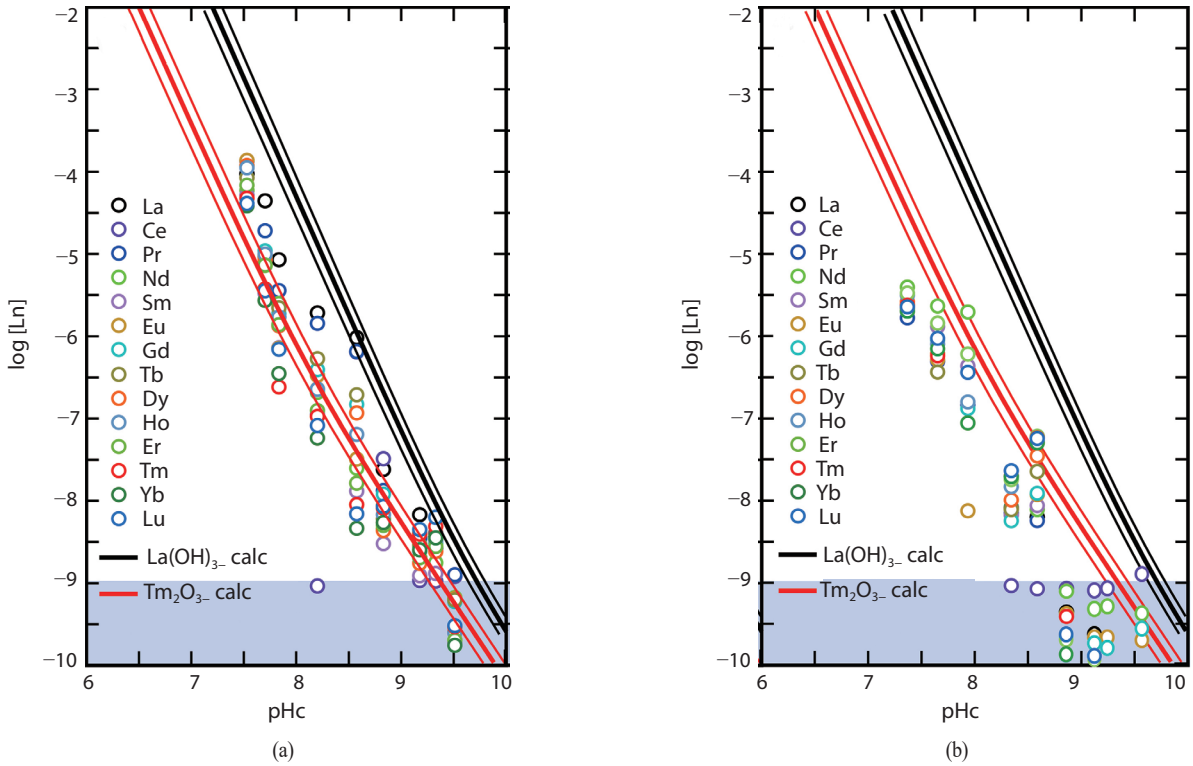

Fig. 4. Ln solubilities of the (a) mixture of the separated pure oxides and (b) the multicomponent Ln_2O_3 mixed oxide solid solution measured at 25°C after aging in the sample solutions for 4 weeks at 60°C, as well as the calculated solubilities of $La(OH)_3$ and Tm_2O_3 at $I = 0.1$ based on the reported thermodynamic constants [19]. The fine curves together with the bold curves represent the maximum and minimum solubility curves calculated from the uncertainty of solubility products. The grey field in the figure indicates the detection limit level of ICP-MS.

as the multicomponent Ln_2O_3 (Ln = La – Lu) mixed oxide, respectively, with the calculated solubilities of pure $La(OH)_3$ and Tm_2O_3 at $I = 0.1$ for comparison. The calculated solubility curves were drawn taking the uncertainty of thermodynamic constants such as solubility product (log $K = -21.7 \pm 0.2$ for $La(OH)_3$ and log $K = -25.2 \pm 0.2$ for Tm_2O_3 [19]) into account as shown in Fig. 4. In Fig. 4(a), the La solubility started from the mixture of separated pure lanthanide oxides was found to be lower than the solubility of $La(OH)_3$ calculated from that aged at 25°C [19]. In the previous study, the solubility of $La(OH)_3$ aged at 90°C was two orders of magnitude lower than that aged at 25°C, suggesting a possible difference on the surface conditions at different aging temperatures [19]. Although such difference was not confirmed after aging at 60°C due to limited number of solubility data [19], the experimental condition of aging at 60°C in the present study might result in lower La solubility compared to that calculated for $La(OH)_3$ aged at 25°C. In contrast, the Tm solubility started from the mixture of separated pure lanthanide oxides was observed to be close to that calculated for Tm_2O_3 aged at 25°C [19]. With a slight decrease in the solubility product from the light to heavy lanthanides, the observed solubility plots also decreased slightly with the increasing atomic number. Notably, the calculated solubility of La_2O_3 [23] was more than 10 orders of magnitude higher than the experimental results in Fig. 4(a), thereby supporting the existence of $La(OH)_3$ as the solubility-limiting solid phase.

The Ln solubilities of the multicomponent Ln_2O_3 mixed oxide (Fig. 4(b)), especially the solubilities of the light lanthanides, were more than one order of magnitude lower than those observed in the mixture of the separated pure

oxides. The XRD pattern revealed the likely formation of the complete solid solution of Ln_2O_3, and the solubility of the light lanthanides might be suppressed by incorporating them into heavier Ln_2O_3 with less solubilities. The measured solubilities of Ce were at the ICP-MS detection level, as shown in Figs. 4(a) and 4(b), indicating that the solubility-limiting solid phase of Ce was CeO_2. Owing to the overlapping of the diffraction peaks of the other lanthanide oxides, further investigations are required to reveal whether CeO_2 was separately formed during the solid-phase synthesis or the contact of the sample solution.

The average mole fractions of the lanthanide [Ln] in the sample solutions in the pH_c range of 7.0–8.5 for the multicomponent Ln_2O_3 mixed oxide and separated pure oxides/hydroxides are summarized in Table 2 and plotted as a function of the reported solubility products of $Ln(OH)_3$ [7] in Fig. 5. The mole fractions of the separated pure oxides/hydroxides increased as the solubility products of $Ln(OH)_3$ increased, except Ce, since its solubility would be controlled by $Ce(III)(OH)_3$, as well as $Ce(IV)O_2$ based on the calculated Pourbaix diagram [24]. The heavy lanthanides, such as Tm, exist as oxides when the experiment started with the contact of each lanthanide oxide with the aqueous solutions, as observed in the previous study [19]. The deviation of the trends of the heavy lanthanides might be caused by the reported solubility product of $Ln(OH)_3$ owing to a lack of the reported values for Ln_2O_3.

Conversely, the average mole fractions of the synthesized multicomponent Ln_2O_3 mixed oxide were almost constant in the lighter to heavier lanthanides. Fig. 3 shows that the multicomponent Ln_2O_3 mixed oxide was synthesized from an equivalent amount of each lanthanide; it likely formed a single-oxide solid solution. Therefore, dissimilar to the separated pure oxides/hydroxides, the constant $x_{Ln,\,aq}$ indicated that the congruent dissolution of the Ln_2O_3 solid solution controlled the apparent solubility behavior of Ln. Fig. 5 shows that $x_{Ln,\,aq}$ exhibited slightly larger values for the heavy lanthanides. This might induce a small deviation in $x_{Ln_2O_3}$ from the light to heavy lanthanides in the oxide-based solid solution. The comparison of the present Ln_2O_3 mixed oxide solid solution to several lanthanide solid solution systems reported in the literature might be interesting. Gausse et al. performed solubility experiments on rhabdophanes ($LnPO_4{\cdot}0.667H_2O$; Ln = La – Dy) and observed the congruent dissolution in a 0.1 M HCl solution and attained equilibrium after approximately 10 days [25]. The slow kinetics observed in this Ln_2O_3 mixed oxide solid solution might be due to the low solubilities under the investigated neutral pH conditions; however, further studies are required to clarify the kinetic effect.

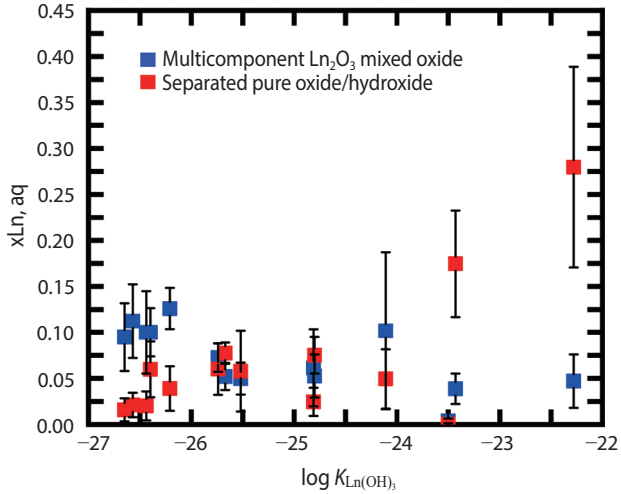

Fig. 5. Mole fraction of each lanthanide in the multicomponent Ln_2O_3 mixed oxide and separated pure oxides/hydroxides, as well as the reported solubility products of $Ln(OH)_3$.

4. Conclusions

Lanthanides, as fission products accumulated in radioactive wastes, can form multicomponent oxide or hydroxide solid solutions under repository conditions. The solubilities of the binary, ternary, and multicomponent lanthanide oxide solid solutions (Ln_2O_3) were studied after aging for four weeks at 60°C. In the binary ((La, Nd) and (La, Eu)) and ternary (La, Nd, Eu) systems in which the solid phases were converted into complete solid solutions of (La, Nd)

$(OH)_3$, (La, Eu)$(OH)_3$, and (La, Nd, Eu)$(OH)_3$, it was observed that the experimental mole fraction of La^{3+} in the aqueous phase was larger than the mole fraction of $La(OH)_3$ in the solid phases, indicating the incongruent dissolution/precipitation of the binary and ternary hydroxide solid solutions. Conversely, in the binary (Eu, Tm) and ternary (La, Eu, Tm) systems in which the initial Tm_2O_3 - based oxide solid solution was retained after contacting the aqueous solutions, the mole fraction of Tm^{3+} in the solution was observed along with the mole fraction of Tm_2O_3 in the solid phases, indicating that the congruent dissolution controlled the solubility behaviors. The thermodynamic analysis based on the total solubility product (ΣΠ) indicated that the solubilities of the hydroxide solid solutions were in thermodynamic equilibrium, while those of the oxide solid solutions were probably dominated by the congruent dissolution. Meanwhile, the XRD pattern of the multicomponent Ln_2O_3 confirmed the formation of the cubic-based oxide solid solution via the incorporation of light lanthanides into heavier Ln_2O_3. The solubility of the lighter lanthanides was suppressed by the formation of the oxide solid solutions with heavier lanthanides, which could be deduced from the solubility behaviors of binary and ternary Ln_2O_3 solid solutions.

Acknowledgements

The authors gratefully acknowledge the financial support from the Japan Society for the Promotion of Science KAKENHI (Grant No. 20H02665).

REFERENCES

[1] I. Grenthe, X. Goana, A.V. Plyasunov, L. Rao, W.H. Runde, B. Grambow, R.J.M. Konings, A.L. Smith, and E.E. Moore. Second Update on the Chemical Thermodynamics of Uranium, Neptunium, Plutonium, Americium and Technetium, OECD/NEA Report, Vol. 14, NEA 7500 (2020).

[2] C. Marquardt, X. Gaona, C. Bube, and M. Altmaier, THEREDA, Thermodynamic Reference Database: Final Report Part KIT-INE, Database for Radionuclides, Karlsruher Institut für Technologie (KIT), Institut für nukleare Entsorgung, Campus Nord (2015).

[3] E. Gifaut, M. Grivé, Ph. Blanc, Ph. Vieillard, E. Colàs, H. Gailhanou, S. Gaboreau, N. Marty, B. Madé, and L. Duro, "Andra Thermodynamic Database for Performance Assessment: ThermoChimie", Appl. Geochem., 49, 225-236 (2014).

[4] A. Kitamura, K. Fujiwara, R. Doi, and Y. Yoshida. Update of JAEA-TDB: Additional Selection of Thermodynamic Data for Solid and Gaseous Phases on Nickel, Selenium, Zirconium, Technetium, Thorium, Uranium, Neptunium Plutonium and Americium, Update of Thermodynamic Data on Iodine, and Some Modifications, Japan Atomic Energy Agency Report, JAEA-Data/Code, 2012-006 (2012).

[5] S.A. Wood, "The Aqueous Geochemistry of the Rare-Earth Elements and Yttrium: 2. Theoretical Predictions of Speciation in Hydrothermal Solutions to 350°C at Saturation Water Vapor Pressure", Chem. Geol., 88(1-2), 99-125 (1990).

[6] I.I. Diakonaov, K.V. Ragnarsdottir, and B.R. Tagirov, "Standard Thermodynamic Properties and Heat Capacity Equations of Rare Earth Hydroxides: II. Ce(III)-, Pr-, Sm-, Eu(III)-, Gd-, Tb-, Dy-, Ho-, Er-, Tm-, Yb-, and Y-hydroxides. Comparison of Thermochemical and Solubility Data", Chem. Geol., 151(1-4), 327-347 (1998).

[7] P.L. Brown and C. Ekberg, Hydrolysis of Metal Ions, Volume 1, Wiley-VCH, Weinheim (2016).

[8] E.D. Fou de Kerdaniel, N. Clavier, N. Dacheux, O. Terra, and R. Podor, "Actinide Solubility-Controlling Phases During the Dissolution of Phosphate Ceramics", J. Nucl. Mater., 362(2-3), 451-458 (2007).

[9] N. Huittinen, Y. Arinicheva, P.M. Kowalski, V.L. Vinograd, S. Neumeier, and D. Bosbach, "Probing Structural

Homogeneity of $La_{1-x}Gd_xPO_4$ Monazite-Type Solid Solutions by Combined Spectroscopic and Computational Studies", J. Nucl. Mater., 486, 148-157 (2017).

[10] Md. Moniruzzaman, T. Kobayashi, and T. Sasaki, "Phase Transformation of Mixed Lanthanide Oxides in an Aqueous Solution", J. Nucl. Radiochem. Sci., 21, 15-27 (2021).

[11] P.D. Glynn and E.J. Reardon, "Solid-Solution Aqueous-Solution Equilibria: Thermodynamic Theory and Representation", Am. J. Sci., 290, 164-201 (1990).

[12] P.D. Glynn, E.J. Reardon, L.N. Plummer, and E. Busenberg, "Reaction Paths and Equilibrium End-Points in Solid-Solution Aqueous-Solution Systems", Geochem. Cosmochim. Acta, 54(2), 267-282 (1990).

[13] P. Glynn, "Solid-Solution Solubilities and Thermodynamics: Sulfates, Carbonates and Halides", Rev. Mineral. Geochem., 40(1), 481-511 (2000).

[14] H. Gamsjäger, E. Königsberger, and W. Preis, "Lippmann Diagrams: Theory and Application to Carbonate Systems", Aquat. Geochem., 6(2), 119-132 (2000).

[15] J. Bruno, D. Bosbach, D. Kulik, and A. Navrotsky. Chemical Thermodynamics of Solid Solutions of Interest in Radioactive Waste Management, OECD/NEA Report, Vol. 10 (2007).

[16] R. Forsyth. An Evaluation of Results From the Experimental Programme Performed in the Studsvik Hot Cell Laboratory, Swedish Nuclear Fuel and Waste Management Co. Report, SKB-TR 97-25 (1997).

[17] S. Zhong and A. Mucci, "Partitioning of Rare Earth Elements (REEs) Between Calcite and Seawater Solutions at 25°C and 1 atm, and High Dissolved REE Concentrations", Geochem. Cosmochim. Acta, 59(3), 443-453 (1995).

[18] L.Z. Lakshtanov and S.L.S. Stipp, "Experimental Study of Europium(III) Coprecipitation With Calcite", Geochem. Cosmochim. Acta, 68(4), 819-827 (2004).

[19] Md. Moniruzzaman, T. Kobayashi, and T. Sasaki, "Solubility and Solid Phase of Trivalent Lanthanide Hydroxides and Oxides", J. Nucl. Radiochem. Sci., 20, 32-42 (2020).

[20] M.H. Nguyen, S.J. Lee, and W.M. Kriven, "Synthesis of Oxide Powders by Way of a Polymeric Steric Entrapment Precursor Route", J. Mater. Res., 14(8), 3417-3426 (1999).

[21] M.A. Gülgün, M.H. Nguyen, and W.M. Kriven, "Polymerized Organic-Inorganic Synthesis of Mixed Oxides", J. Am. Ceram. Soc., 82(3), 556-560 (1999).

[22] V. Neck, M. Altmaier, T. Rabung, J. Lützenkirchen, and T. Fanghänel, "Thermodynamics of Trivalent Actinides and Neodymium in NaCl, $MgCl_2$, and $CaCl_2$ Solutions: Solubility, Hydrolysis, and Ternary Ca–M(III)–OH Complexes", Pure Appl. Chem., 81(9), 1555-1568 (2009).

[23] R.J.M. Konings, O. Beneš, A. Kovács, D. Manara, and D. Sedmidubsky, "The Thermodynamic Properties of the F-Elements and Their Compounds. Part 2. The Lanthanide and Actinide Oxides", J. Phys. Chem. Ref. Data, 43(1), 013101 (2014).

[24] I. Puigdomenech, "HYDRA (Hydrochemical Equilibrium- Constant Database) and MEDUSA (Make Equilibrium Diagrams Using Sophisticated Algorithms) Programs," Royal Institute of Technology, Sweden. Accessed Jun. 24 2021. Available from: http://www.ke- mi.kth.se/medusa.

[25] C. Gausse, S. Szenknect, D.W. Qin, A. Mesbah, N. Clavier, S. Neumeier, D. Bosbach, and N. Dacheux, "Determination of the Solubility of Rhabdophanes $LnPO_4 \cdot 0.667H_2O$ (Ln = La to Dy)", Eur. J. Inorg. Chem., 4615-4630 (2016).